

# Spatial Variability in the Ratio of Interstellar Atomic Deuterium to Hydrogen. I. Observations toward $\delta$ Orionis by the Interstellar Medium Absorption Profile Spectrograph

Edward B. Jenkins, Todd M. Tripp, Przemysław R. Woźniak,  
Princeton University Observatory, Princeton, NJ 08544

Ulysses J. Sofia<sup>1</sup>

Department of Astronomy and Astrophysics, Villanova University, Villanova, PA 19085

and

George Sonneborn

Code 681, NASA Goddard Space Flight Center, Greenbelt, MD 20771

## ABSTRACT

Studies of the abundances of deuterium in different astrophysical sites are of fundamental importance to answering the question about how much deuterium was produced during big bang nucleosynthesis and what fraction of it was destroyed later. With this in mind, we used the Interstellar Medium Absorption Profile Spectrograph (IMAPS) on the ORFEUS-SPAS II mission to observe at a wavelength resolution of  $4 \text{ km s}^{-1}$  (FWHM) the  $L\delta$  and  $L\epsilon$  absorption features produced by interstellar atomic deuterium in the spectrum of  $\delta$  Ori A. A  $\chi^2$  analysis indicated that  $0.96 < N(\text{D I}) < 1.45 \times 10^{15} \text{ cm}^{-2}$  at a 90% level of confidence, and the gas is at a temperature of about 6000K. In deriving these results, we created a template for the velocity profile defined by 7 different N I transitions recorded at a high signal-to-noise ratio. Extra free parameters in the analysis allowed for the additional uncertainties that could arise from various sources of systematic error.

To derive a value for D/H, we measured the  $L\alpha$  absorption features in 57 spectra of  $\delta$  Ori in the IUE archive, with the objective of arriving at a more accurate H I column density than those reported by other investigators. From our measurement of  $N(\text{H I}) = 1.56 \times 10^{20} \text{ cm}^{-2}$ , we found that  $N(\text{D I})/N(\text{H I}) = 7.4_{-1.3}^{+1.9} \times 10^{-6}$  (90% confidence). Systematic errors in the derivation of  $N(\text{H I})$  probably dominate over the very small formal error, but

---

<sup>1</sup>Present address: Dept. of Astronomy, Whitman College, 345 Boyer Ave., Walla Walla, WA 99362.

their relative value should be smaller than that for  $N(\text{D I})$ . Our result for  $\text{D}/\text{H}$  contrasts with the more general finding along other lines of sight that  $\text{D}/\text{H} \approx 1.5 \times 10^{-5}$ . The underabundance of D toward  $\delta$  Ori A is not accompanied by an overabundance of N or O relative to H, as one might expect if the gas were subjected to more stellar processing than usual.

*Subject headings:* ISM: Abundances — ISM: Atoms — Ultraviolet: ISM

## 1. Introduction

The relative abundances of the light elements not only substantiate the standard interpretation for Big Bang Nucleosynthesis<sup>2</sup> (BBN) (Reeves et al. 1973; Epstein, Lattimer, & Schramm 1976), but they also hold the key for our determining the universal ratio of baryons to photons, commonly designated by the parameter  $\eta$  (Boesgaard & Steigman 1985; Olive et al. 1990; Smith, Kawano, & Malaney 1993). There has been considerable interest in measuring the abundance of deuterium, since its production was strongly regulated by photodestruction in the radiation bath during the BBN, making  $\text{D}/\text{H}$  a strong discriminant of  $\eta$ .

Deuterium is also destroyed in stars. After having passed through one or more generations of stars, diffuse gases that we can observe have probably had their deuterium abundances reduced to values below those that result from BBN. Thus it is important to observe systems that have different levels of chemical enrichment and mixing (Timmes et al. 1997), so that we can untangle the effects of the two fundamental destruction mechanisms, i.e., the photodestruction accompanying BBN and the astration of material as the universe matures. A key step in this area of research is to form a solid foundation of measurements of D in the chemically evolved gas in the disk of our Galaxy. Ultimately, when these results are combined with determinations for distant gas systems that have not aged as much, we expect to achieve a better understanding about the processing of gas through stars, which is interesting in its own right (Steigman & Tosi 1992, 1995; Dearborn, Steigman, & Tosi 1996; Scully et al. 1997; Tosi et al. 1998), and this in turn should allow us to extrapolate the concentration of D back to an era very soon after its primordial production.

An important foundation in recognizing the relationship between  $\text{D}/\text{H}$  and some measure of stellar processing, such as the relative abundances of elements produced in

---

<sup>2</sup>However see Gnedin & Ostriker (1992) and Burbidge & Hoyle (1998) for contemporary viewpoints that differ from this interpretation.

stellar interiors, is that an empirical relationship between the two forms a unique sequence. If this turns out not to be true, then more elaborate interpretations of chemical evolution may be needed. To explore this issue, we have embarked on a program to revisit some lines of sight studied by other investigators (§2), but this time using much higher resolution spectra obtained with the Interstellar Medium Absorption Profile Spectrograph (IMAPS).

In this paper, we investigate the spectrum of  $\delta$  Ori A (HD 36486). This star has a spectral classification of O9.5 II, is a spectroscopic binary, and is a member of the Ori OB1 association that has a distance modulus of 8.5 ( $d = 500$  pc) (Humphreys 1978). In a companion paper (Sonneborn et al. 1999) we will report on results for  $\gamma^2$  Vel and  $\zeta$  Pup. The basic properties of our spectrum of  $\delta$  Ori and the instrument that recorded it are discussed in §3.1, followed by examinations of systematic errors that could arise in the determination of a very weak contamination signal (§3.2), the intensity of the scattered light background (§3.3), and absorption features from other species (§3.4). In §4.1 we describe how we obtained independent information on the shape of the velocity profile for material toward  $\delta$  Ori, so that we could undertake our study with only a small number of unknown, free parameters. We have paid considerable attention to minimizing the errors and evaluating them in a fair and consistent manner (§4.2). For our value of  $N(\text{D I})$  reported in §4.3 to be useful, we must compare it with  $N(\text{H I})$ , and we must strive to make the accuracy of the latter as good as or better than the former. In §5 we discuss our comprehensive investigation of the IUE archival data that show  $\text{L}\alpha$  absorption in the spectrum of  $\delta$  Ori. This special analysis combined with our determination of  $N(\text{D I})$  ultimately led to our determination of the atomic D/H toward  $\delta$  Ori reported in §6. We relate this result to the abundances of other elements relative to H in §7 and discuss its significance in §8.

## 2. Previous Measurements of Atomic D/H in the Galaxy

Early measurements of D/H obtained from the *Copernicus* satellite (resolution  $15 \text{ km s}^{-1}$  FWHM) and IUE (resolution  $25 \text{ km s}^{-1}$  FWHM), summarized by Vidal-Madjar & Gry (1984), had a few cases that differed by more than the reported errors from a general average  $\text{D/H} \approx 1.5 \times 10^{-5}$ . At face value, this suggested that D/H varies from one location to the next. McCullough (1992) revisited this problem and asserted that the evidence for such variations was not convincing. In making his claim that all of the data were consistent with a constant value for D/H, McCullough rejected all of the deviant cases on the grounds that the complexity of their velocity structures made the measurements much less accurate than originally claimed.

The high resolution ( $2.5 \text{ km s}^{-1}$  FWHM) and good sensitivity of the GHRS instrument on HST enabled an accumulation of very accurate observations of the interstellar  $\text{L}\alpha$  H and D absorption features superposed on the broader chromospheric  $\text{L}\alpha$  emission lines of nearby F, G and K type stars. The best determinations of D/H were those toward  $\alpha$  Aur (Capella), where Linsky, et al. (1995) found that  $\text{D}/\text{H} = 1.60_{-0.19}^{+0.14} \times 10^{-5}$ , and toward HR 1099, where Piskunov, et al. (1997) obtained  $\text{D}/\text{H} = 1.46 \pm 0.09 \times 10^{-5}$ . The issue of whether or not atomic deuterium to hydrogen ratios toward other cool stars differ from these values has been an elusive one, although it seems clear that one could rule out deviations greater than about 50% in either direction (Wood, Alexander, & Linsky 1996; Dring et al. 1997; Piskunov et al. 1997). The chief problem has been that the measurements of  $N(\text{H I})$  toward late-type stars were very dependent on assumptions about the shape of the underlying emission profile (Linsky & Wood 1996; Piskunov et al. 1997) or the compensations for additional, broad absorptions caused by hydrogen walls associated with the stellar wind cavities around either the Sun or the target stars (Linsky & Wood 1996; Wood & Linsky 1998). Even so, these investigations revealed some intriguing, convincing variations for the abundances of D I with respect to those of Mg II. Unfortunately, the significance of these changes is clouded by the possibility that they could result simply from alterations in the amount of depletion of Mg onto dust grains (Murray et al. 1984; Jenkins, Savage, & Spitzer 1986; Sofia, Cardelli, & Savage 1994; Fitzpatrick 1997).

Lemoine, et al (1996) observed the interstellar H and D  $\text{L}\alpha$  absorption features in the spectrum of the DA white dwarf G191–B2B with the GHRS and reported their determinations for D/H. Later, high-resolution observations by Vidal-Madjar, et al (1998) brought forth some refinements in the interpretation of the velocity structures of the absorption profiles, leading to a determination  $\text{D}/\text{H} = 1.12 \pm 0.08 \times 10^{-5}$  for all of the material in front of this star. If one allows for the fact that a contribution from the Local Interstellar Cloud (LIC) is somewhat blended with those of more distant clouds and adopts the  $\alpha$  Aur result for the LIC, D/H toward the other material could be of order  $9 \times 10^{-6}$ . This low value for D/H is supported by observations of the hot subdwarf BD +28°4211 reported by Götz, et al. (1998),  $\text{D}/\text{H} = 8_{-4}^{+7} \times 10^{-6}$ , although the error bar is large enough to include the results obtained for  $\alpha$  Aur, HR 1099, and other late-type stars.

For lines of sight that have hydrogen column densities that are small enough to analyze using the  $\text{L}\alpha$  profile, there is the danger that improper allowances for either  $\text{L}\alpha$  emission (cool stars) or absorption (hot dwarfs) could lead to errors. Moreover, in some circumstances hydrogen walls associated with either the target stars or the Sun can lead to complications. One way to bypass these problems is to examine the higher Lyman series absorption features toward more distant, early-type stars with much more foreground material, as was done with the *Copernicus* satellite. We also have the benefit of sampling

the interstellar medium well outside our immediate vicinity. However, a principal weakness of *Copernicus* was its limited resolving power ( $\approx 15 \text{ km s}^{-1}$  FWHM).<sup>3</sup> In large part, the *Copernicus* investigators had to model the instrumentally smeared, detailed velocity structure of the gas, with guidance from high-resolution observations of Na I features recorded from the ground. Unfortunately, the sodium D lines are a poor standard for comparison because their strengths are dependent on ionization equilibria that are entirely different from those of D I and H I. In this study we revisit the case for  $\delta$  Ori, originally observed with *Copernicus* by Laurent, et al. (1979), but now with new observations taken with an instrument with considerably better velocity resolution than *Copernicus*.

### 3. Observations and Data Reduction

#### 3.1. Basic Properties of the Spectra

A far-UV spectrum of  $\delta$  Ori over the wavelength interval 930 to 1150 Å was recorded in a series of exposures lasting 54 min over various observing intervals between 22 November and 3 December 1996 by the Interstellar Medium Absorption Profile Spectrograph (IMAPS). This series of observations was undertaken during the ORFEUS-SPAS II mission (Hurwitz et al. 1998) on STS-80, which was the second orbital flight of IMAPS. IMAPS is a simple, objective-grating echelle spectrograph that can record the far-UV spectrum of a bright, early-type star with sufficient resolution to show many of the velocity structures in the interstellar lines. Jenkins, et al. (1996) present a detailed description of the IMAPS instrument, its performance on the first ORFEUS-SPAS mission in 1993<sup>4</sup>, and the methods of data correction and analysis.

We summarize very briefly how the spectra are recorded by IMAPS: In any single exposure that covers an angle  $18'20'' \times 14'40''$ , one-quarter of the echelle grating’s free spectral range and, nominally, diffraction orders 194 through 242 are recorded by an electron-bombarded CCD image sensor. This detector has an opaque photocathode on a smooth substrate and uses magnetic focusing to form the electron image on the CCD.

---

<sup>3</sup>Another drawback with *Copernicus* was that all observations had to be taken in sequence, since the spectrometer was a scanning instrument. Vidal-Madjar, et al. (1982) obtained inconsistent results for different Lyman series lines in the spectrum of  $\epsilon$  Per, an effect which they attributed to the influence of stellar features that varied with time.

<sup>4</sup>Improvements in IMAPS after the first flight removed most of the problems discussed by Jenkins, et al. (1996; in particular, see their §8.2). Most important, the severe changes in photocathode sensitivity that were evident on the first flight were not manifested on the second flight.

Electrons impacting on the back side of the specially thinned CCD have an energy of 18 keV, and they produce enough secondary electrons within the silicon layer to make individual photoevents appear as bright spots. Each spot has an amplitude that is about 20 times greater than the combined noise from the readout amplifier and the random fluctuations in dark current. The CCD has a format of  $320 \times 256$  pixels, each of which is  $30\mu\text{m}$  square and subtends a  $\Delta\lambda$  equivalent to a Doppler shift of  $1.25\text{ km s}^{-1}$ . The echelle orders are separated by about 5 CCD pixels, but they are rather broad in the cross-dispersion direction. The CCD is read out 15 times a second. The video signals from successive frames are summed in an accumulating memory to produce the integrated spectral images. In our processing of these images after the flight, we subtracted dark-current comparison frames that were recorded at frequent intervals with the accelerating high voltage turned off.

The effective area of IMAPS on the 1996 flight was about  $3\text{ cm}^2$  at wavelengths longward of about  $1020\text{ \AA}$ , leading to typical signal-to-noise ratios of about 80 near the maximum of the echelle grating’s blaze angle for stars as bright as  $\delta\text{ Ori A}$ . However the Al+LiF coatings on the two gratings have a low reflection efficiency at shorter wavelengths, resulting in a factor of 10 lower effective area in the vicinity of the  $\text{L}\delta$  and  $\text{L}\epsilon$  lines. This reduced efficiency coupled with the much lower flux at the centers of the stellar Lyman series lines made it especially difficult to achieve high values of signal-to-noise. We overcame this problem by recording a large number of spectra that could be added together. The total integrated flux at the continuum levels near  $\text{L}\delta$  and  $\text{L}\epsilon$  amounted to about 600 photons for each CCD pixel width in the dispersion direction ( $1.25\text{ km s}^{-1}$ ). Noise fluctuations in the spectra had *rms* deviations about equal to 1/10 of the continuum levels, with the principal noise source being the multiple readouts of the CCD, rather than from photon-counting statistical errors. (This is clearly evident in Fig. 1, which shows a noise level at zero intensity to be about the same as that at the elevated intensity levels.)

We deliberately introduced offsets in position for the spectra in different sets of exposures. This was done to reduce the possibility that the spectrum could be perturbed by subtle flaws, such as CCD columns with anomalous responses or variations in photocathode efficiency with position (we could see no evidence for the latter however).

Figure 1 shows the D and H absorption profiles for  $\delta\text{ Ori}$  at  $\text{L}\delta$  and  $\text{L}\epsilon$ . Observations of telluric atomic oxygen lines from excited fine-structure levels, seen elsewhere in the IMAPS spectrum of this star, indicated that the instrumental profile that governs the wavelength resolution of these observations was consistent with a Gaussian distribution having a FWHM<sup>5</sup> equal to  $4.0\text{ km s}^{-1}$ . At this resolving power, the deuterium features are well

---

<sup>5</sup>See Jenkins & Peimbert (1997) for the details on how to arrive at this finding – their measurements for

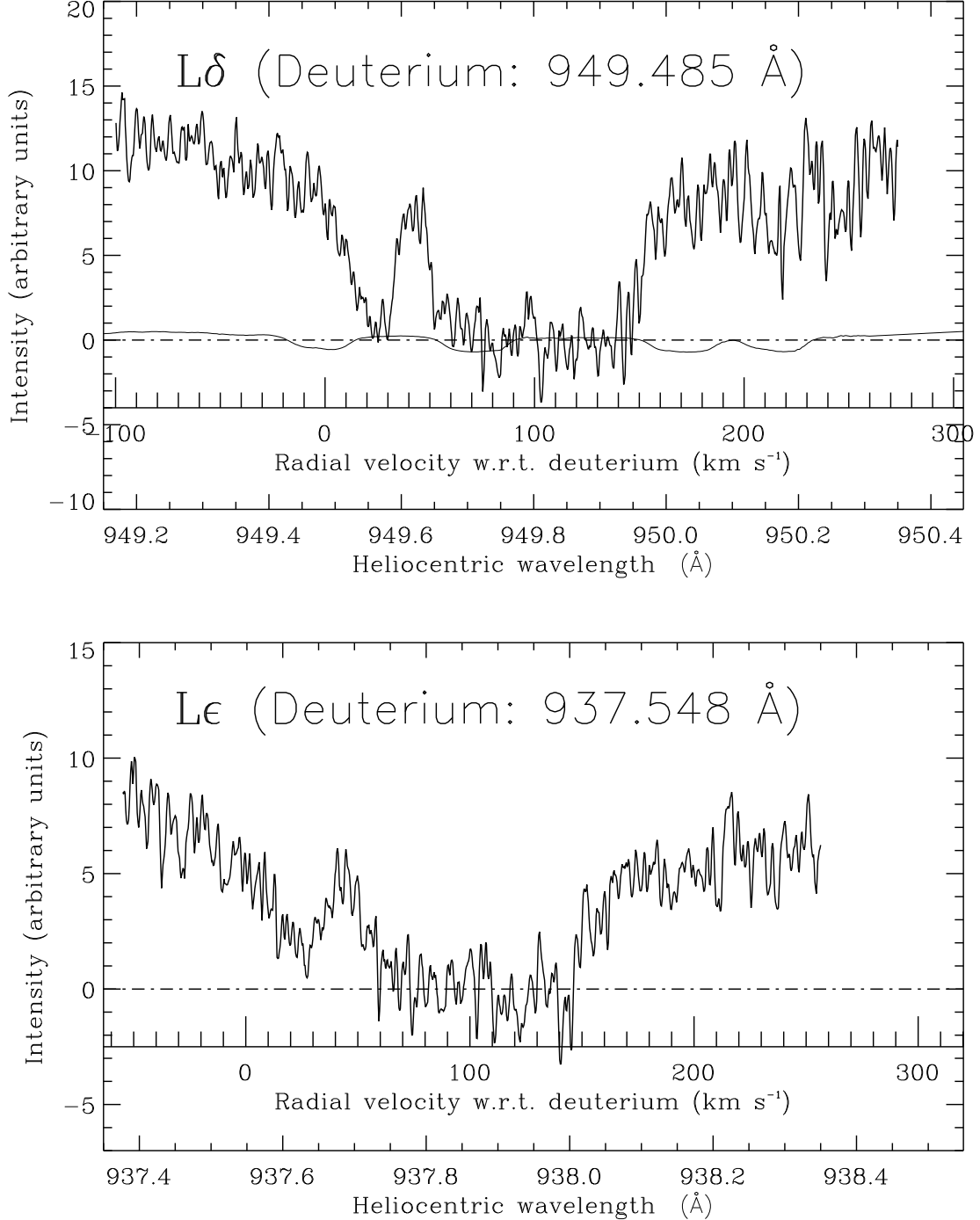


Fig. 1.— The D and H absorption features at L $\delta$  and L $\epsilon$  in the IMAPS spectrum of  $\delta$  Ori, shown with a sampling interval of  $1/2$  CCD pixel (§3.1). In both cases, the velocity scale refers to the D feature in the heliocentric reference frame. For L $\delta$ , the character and amplitude of a correction (§3.2) for possible contamination from features in an adjacent order is shown (line that oscillates on either side of the zero level), with a scale factor  $R_c = 0.0070$  (best fits came out over the range 0.0058 to 0.0080 for the largest extremes shown in Table 2). The spectra are also corrected for the small effects arising from interfering lines (§3.4).

separated from their hydrogen counterparts, as can be seen in Fig. 1. While the deuterium  $L\delta$  profile does show some asymmetry, to within the uncertainties of the noise there does not seem to be any extraordinary complexity in the velocity structure of the D profiles. For instance, there seems to be no evidence for any strong, narrow velocity components buried within the main peak of the  $L\epsilon$  feature. Most important, the D features are not badly saturated.

### 3.2. Possible Contamination Signal

There is some overlap of signal from one echelle diffraction order to the next. Our optimal extraction routine was designed to compensate for this effect (Jenkins et al. 1996), but if this correction was not perfect we may have had some contamination by the spectral intensities from an adjacent order. We had to be especially watchful for this possibility in the vicinity of the Lyman series lines because the stellar continuum level in the region of interest is much lower than elsewhere. This gives the contamination signal an advantage over the signal we wished to study. For  $L\epsilon$  there is no problem because there are no spectral features in the orders either directly above or below the D and H features or their nearby continua. Errors in correcting for order overlap will only change the effective zero intensity level, which is corrected out anyway. The next higher order of diffraction that appears just below the one that contains the  $L\delta$  absorptions is featureless, but, unfortunately, the order above the  $L\delta$  order exhibits interstellar absorption features from the very strong multiplet of N I at 954 Å.

In our investigation of the spectrum in the vicinity of  $L\delta$ , we allowed for the possibility that our correction for the order overlap was either too large or too small. This error could have added a spurious signal to our spectrum. Therefore, we included as a free parameter a scaling coefficient  $R_c$  (which could be either positive or negative) for the amplitude of a correction signal (with the same shape) to cancel the possible residual contamination, and we allowed it to vary as we explored for minimum values of  $\chi^2$  (§§ 4.2 and 4.3). When this coefficient is less than 0.005 or larger than 0.03, unreasonably large perturbations can be seen in the bottom of the very broad hydrogen feature. Within this range, however, we allowed for the fact that our derivation of  $N(\text{D I})$  could be influenced by the exact value. Figure 1 shows the correction signal with the most plausible amplitude, as indicated by minimum  $\chi^2$  for  $R_c$  at the most probable  $N(\text{D I})$  given in Table 2. The spectrum that is shown in this figure has had this correction included.

---

the IMAPS spectrum of  $\zeta$  Ori A are not far from those that apply to our  $\delta$  Ori spectrum.



### 3.3. Background Level

Our analysis of the D profiles is very dependent on our having an accurate determination of the level of zero intensity. Sources of background illumination include not only grating scatter, but also a diffuse glow caused by a portion of the  $L\alpha$  geocoronal background that is not fully rejected by a mechanical collimator at the instrument’s entrance aperture. (The detector’s dark count rate is negligible compared to these sources of background.) Fortunately, we could use the bottoms of the broad, heavily saturated H absorptions that accompany each D profile establish the position of the background level.

In principle, the saturated portion of the H profile could mislead us if there were broad, shallow wings in the instrumental profile caused by scattering from the echelle grating. If this were the case, one could imagine that the local background level might increase slightly for wavelengths somewhat removed from the strong H feature. We can rule out this prospect on two grounds. First, before IMAPS was flown, we illuminated it in a vacuum tank with a collimated beam from a molecular hydrogen emission line source, and faint, very broad wings of the recorded emission lines could be seen only on the strongest features. The energy in these wings corresponded to 15% of the total, spread over several Å. The remaining 85% was within the main peak. Second, for  $\delta$  Ori we found that for both  $L\delta$  and  $L\epsilon$  the apparent depths of the D features in *Copernicus* scans (taken with an ordinary grating in first order) showed excellent agreement with those registered in the IMAPS spectrum after it had been degraded by convolving it with the *Copernicus* instrumental profile function [a triangle with  $\text{FWHM} = 0.045 \text{ Å}$  (Laurent, Vidal-Madjar, & York 1979)]. For these two reasons, we feel confident that the apparent flux in the bottom of the H feature is, to within the uncertainties from noise, a good representation for the zero level under the deuterium line.

### 3.4. Interference from Other Lines

Table 1 lists lines from species other than D I and H I that are in vicinity of the deuterium absorptions or the fragments of the spectrum that were used to define the continuum level (§4.3). The Werner 3–0 P(2) line lies within the H  $L\delta$  feature, and thus it is of no importance. From other lines out of the  $J=4$  level of  $\text{H}_2$  that appear elsewhere in our IMAPS spectrum, we know that the 4–0 P(4) line of the Werner system should have a negligible strength. Again using other features in the IMAPS spectrum, we found that the remaining two lines shown in the table could perturb our spectra and influence our final results. We therefore felt it was necessary to estimate their strengths and then apply a correction to compensate for their presence.

Table 1. Lines in the Vicinity of Deuterium  $L\delta$  and  $L\epsilon$

Identification	$\lambda^a$ (Å)	$\log f\lambda^b$	Comment
H <sub>2</sub> Werner 3–0 P(2)	949.608	–0.078	Within the $L\delta$ H I absorption
H <sub>2</sub> Lyman 14–0 P(2)	949.351	0.95	On cont. left of the $L\delta$ D I absorption
Fe II . . . . .	937.652	1.263	On cont. between $L\epsilon$ D I and H I absorptions
H <sub>2</sub> Werner 4–0 P(4)	937.551	0.89	Too weak to matter

<sup>a</sup>The H<sub>2</sub> Lyman lines are from Abgrall et al. (1993a), the Werner lines are from Abgrall et al. (1993b) and the Fe II line is from Morton (1991). The maximum absorptions should occur at a Doppler shift of about +23 to +25 km s<sup>–1</sup> with respect to the heliocentric wavelength scales shown in Fig. 1.

<sup>b</sup>All of the H<sub>2</sub> lines are from Abgrall & Roueff (1989) and the Fe II line is from Morton (1991).

To estimate the strength of the 14–0 P(2) Lyman line of H<sub>2</sub>, we noted that the 4–0 R(2) line at 1051.498 Å had a maximum depth of 0.27 times the local continuum at  $v = 23 \text{ km s}^{-1}$ , and it was recorded in a part of our spectrum where the signal-to-noise ratio was about 80. This line has a value for  $f\lambda$  that is 1.7 times that of the 14–0 P(2) line. To compensate for the effect of the latter on our continuum to the left of the D I L $\delta$  feature, we divided the observed spectrum by the continuum-normalized intensities in Lyman 4–0 R(2) profile all taken to the 1/1.7 power, with the profile shifted in wavelength to match that of the 14–0 P(2) line.

For a template of the Fe II absorption, we used the line at 1081.875 Å that shows a maximum depth of 0.26 at  $v = 25 \text{ km s}^{-1}$  recorded at S/N = 90 (this maximum for the 937.652 Å line falls within the H absorption) and a shoulder at  $v = 12 \text{ km s}^{-1}$  with a depth of 0.12. This shoulder for the 937.652 line falls on top of a critical piece of continuum between the D I and H I L $\epsilon$  features. The 1081.875 line has  $f\lambda$  that is 0.82 times that of the interfering feature (Morton 1991), and once again this difference was taken into account when we made the correction.

## 4. Interpretation of the Data

### 4.1. Velocity Profile Template

To derive the most accurate value for the column density of atomic deuterium  $N(\text{D I})$ , it is beneficial to use information from other species recorded at much higher S/N to help define more accurately the shape of the D I velocity profile. Profiles of O I and N I are probably the most suitable comparison examples for two reasons. First, these two elements have very mild depletions, if any, caused by the atoms condensing into solid form onto dust grains (Meyer, Cardelli, & Sofia 1997; Meyer, Jura, & Cardelli 1998). The column densities of N and O seem to track those of H over a diverse sample of regions (Ferlet 1981; York et al. 1983). As a consequence, it is unlikely that their velocity profiles will differ appreciably from that of D I. This is in contrast to the usual striking differences exhibited between elements that are mildly depleted, such as Na I, and elements that are strongly depleted, such as Ca II. The former is generally concentrated at lower velocities than the latter for a given line of sight (Routly & Spitzer 1952; Siluk & Silk 1974; Vallergera et al. 1993; Sembach & Danks 1994). Second, O I and N I have ionization potentials close to that of neutral hydrogen, and this close match in energy makes their susceptibility to ionization nearly the same and also insures that the cross sections for (nearly resonant) charge exchange are high (Field & Steigman 1971; Butler & Dalgarno 1979). For this reason, plus the consideration that whatever means there are for ionizing N and O will operate in much the same way

for H (or D), we can generally regard the relative ionizations of oxygen and nitrogen to be good representations for that of D [but for evidence to the contrary, see Vidal-Madjar et al. (1998)]. This assumes, of course, that O and N are not being ionized appreciably to multiply charged states.<sup>6</sup>

In the wavelength coverage of IMAPS where we have a reasonably good S/N, there are no transitions from the O I ground state that are weak enough (and with known f-values) to yield absorption lines that we can analyze. There is, however, a good series of exposures in the HST archive<sup>7</sup> that cover the O I 1355.6 Å feature in the spectrum of  $\delta$  Ori, recorded by the GHRS Echelle-A spectrograph. Unfortunately, the transition probability for this line is so weak that only the main peak in the velocity profile shows up above the noise.

For N I, within the coverage of IMAPS there are three multiplets (at 952.4 Å, 953.8 Å and 954.1 Å) from the ground level that are ideal for studying the apparent distribution<sup>8</sup>  $N_a(v)$  of the nitrogen atoms with velocity, defined as

$$N_a(v) = 3.768 \times 10^{14} \frac{\tau_a(v)}{f\lambda} \text{cm}^{-2} (\text{km s}^{-1})^{-1}, \quad (1)$$

where the apparent optical depth  $\tau_a(v)$  is a valid quantity to measure at velocities  $v$  where the line is not badly saturated or, alternatively, not too weak. In this equation  $f$  is the transition’s oscillator strength, and  $\lambda$  is expressed in Å. In our study of the N I lines, we adopted f-values from the laboratory measurements of Goldbach, et al. (1992). For the triplet at 952.4 Å, the weakest feature at 952.523 Å is only moderately saturated. The other two features are heavily saturated but useful for revealing the weaker shoulder on the left-hand side of the main peak. The 4 much stronger features of N I in the vicinity of 954 Å are useful for defining accurately the behavior of  $N_a(v)$  at velocities where it is below about  $5 \times 10^{13} \text{cm}^{-2} (\text{km s}^{-1})^{-1}$ . We derived a composite  $N_a(v)$  profile for N I from the 7 lines using the method employed by Jenkins & Peimbert (1997) when they synthesized the profiles of H<sub>2</sub> in various  $J$  levels toward  $\zeta$  Ori A.

Figure 2 shows the  $N_a$  profiles that we derived for N I and O I. We chose to work with the N I profile in our interpretation of the D lines because it was of much better quality.

---

<sup>6</sup>We looked for absorption by the N III transition at 989.799 Å in our IMAPS spectrum of  $\delta$  Ori A. No absorption was evident at  $v = 25 \text{ km s}^{-1}$ , but it was difficult to assign a quantitative upper limit because of interference from the nearby feature of Si II at 989.873 Å.

<sup>7</sup>Exposure identifications z2zb0304t, z2zb0305t and z2zb0306t.

<sup>8</sup>For the distinction between the *apparent* and *true* velocity distributions, see the discussions by Savage & Sembach (1991) and Jenkins (1996). In our study of  $\delta$  Ori at high velocity resolution, it is probably safe to assume that the two are equal to each other.

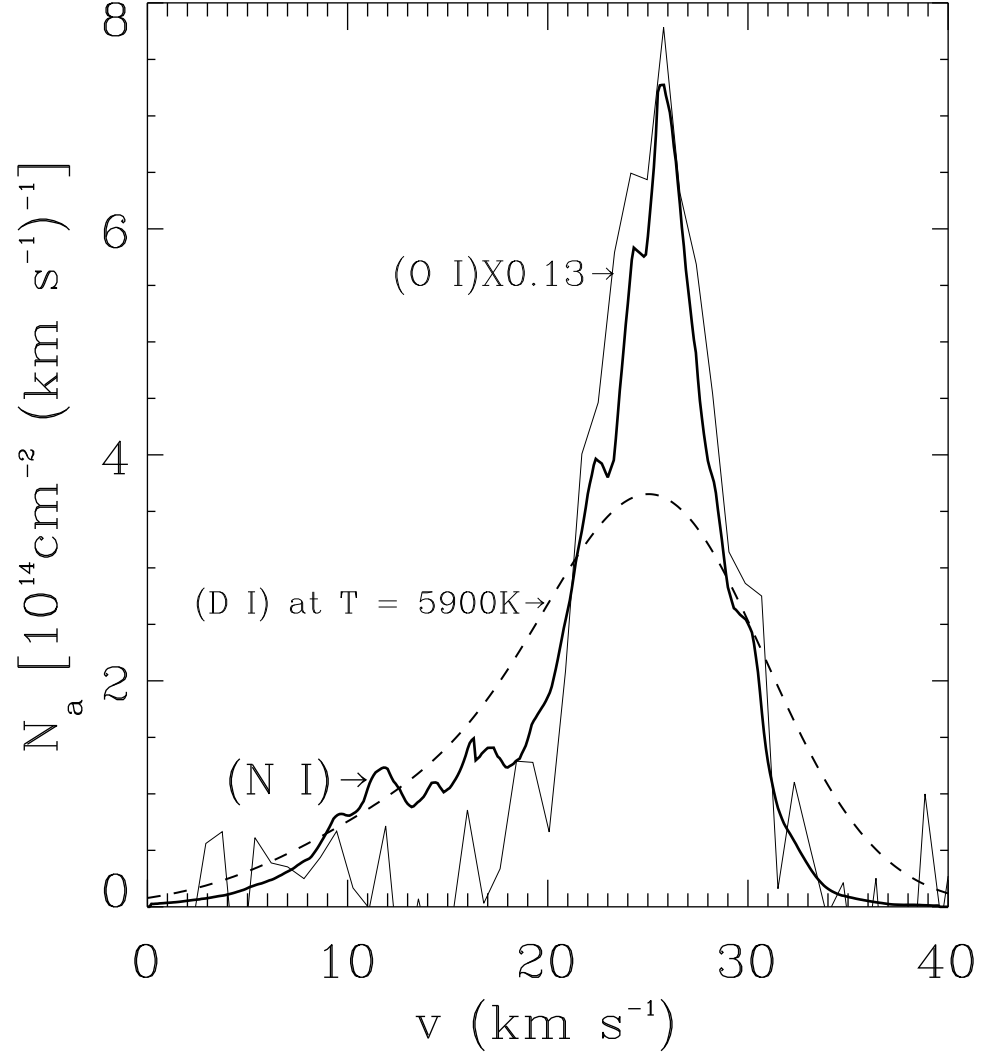


Fig. 2.— Profiles for  $N_a(v)$  for N I (heavy line) and O I (light line), recorded by IMAPS and HST, respectively. The dashed line shows the expected shape of the deuterium profile for an additional thermal broadening at  $T = 5900\text{K}$  (see Eq. 3) of the N I profile favored by our most likely solution in Table 2.

This pragmatic reason for choosing N I as a template is contrary to the idealistic stance that O I would be a better match to D I, based on evidence from the absorption lines in the spectrum of G191-B2B recorded by Vidal-Madjar, et al (1998) and calculations of partially ionized atomic gases by Sofia & Jenkins (1998). We note, however, that to within the noise fluctuations the significant part of the profile of O I is consistent with the main part of the profile of N I. There is a suggestion of an apparent inconsistency between N I and O I in the velocity range  $10 < v < 20 \text{ km s}^{-1}$ . While this may be true, we point out that this weak shoulder in the O I absorption, if it exists, may have been lost in the fitting of the continuum to the curvature of the stellar spectrum, which is larger than the expected size of the shoulder indicated by the N I profile. Also, the existence of some absorption to the left of a main peak is supported by the shape of the L $\delta$  deuterium profile shown in Figures 1 and 3.

In principle, we should be cautious about possible contamination of the interstellar N I profile by nitrogen atoms in the Earth’s atmosphere above our orbital altitude of 295 km. Above this altitude, the MSIS-86 model atmosphere for solar minimum shows an exponential decrease in the density of nitrogen atoms with a scale height of 53 km, starting at a density of  $5.5 \times 10^6 \text{ cm}^{-3}$  at 295 km (Meier 1991). For a zenith angle  $z$  of  $45^\circ$ , we calculate that the telluric contribution to the observed  $N(\text{N I})$  should be  $1.3 \times 10^{13} \text{ cm}^{-2}$ , an amount that would be just about invisible in the representation shown in Fig. 2. Even at  $z = 90^\circ$ ,  $N(\text{N I}) = 1.3 \times 10^{14} \text{ cm}^{-2}$ , which is just slightly larger than the bump (presumably due to noise) immediately to the right of the “(N I) $\rightarrow$ ” indication in the figure. Thus, we feel it is safe to dismiss the possibility that any telluric N I contamination is large enough to influence our profile.

One important difference between D and either N or O is the atomic mass. If the thermal Doppler broadening for deuterium atoms is not very much less than that due to macroscopic motions, we would expect the D profiles to be broader than those of O and N. With the simplifying assumption that the temperature of the gas does not vary much from place to place, we expect that for nitrogen the observed distribution of the atoms with velocity is represented by the turbulent motions  $t(v)$  convolved with the thermal Doppler profile,  $\phi_D(m, T, v)$ , given by

$$\phi_D(m, T, v) = \sqrt{m/(2\pi kT)} \exp[-mv^2/(2kT)] , \quad (2)$$

with  $m$  equal to 14 times the proton mass  $m_p$ . For convenience, we can include in  $t(v)$  the instrumental smearing of the profile, on the condition that we are not being misled by saturated, unresolved structures in the absorption line (Savage & Sembach 1991; Jenkins 1996). The same relation holds for deuterium with  $m = 2m_p$ . Since the convolution of two Gaussian distributions produces a third with a second moment equal to the sum of the two

original ones, we can state that

$$t(v) * \phi_D(2m_p, T, v) = t(v) * \phi_D(14m_p, T, v) * \phi_D(7m_p/3, T, v) . \quad (3)$$

When we analyzed the deuterium features, we adopted for a standard model of their shapes the nitrogen velocity profile convolved with the last term in Eq. 3. We allowed the temperature  $T$  to be a free parameter that could influence the fit between the profiles of N I and D I (and one that is also of some astrophysical relevance). We did not allow for variations of  $T$  among unrecognized and blended velocity substructures that contributed to the profile, since the identification of these components is somewhat arbitrary. Our goal was to account for the general modification of the profile due to the known differences in the effects of thermal and turbulent broadening. (For determining  $N(\text{D I})$ , the weakness of the dependence of the derived  $N(\text{D I})$  with  $T$  expressed in the endnote of Table 2 indicates that our simplification that  $T$  is constant is probably safe.) Figure 2 shows our model for the deuterium profile (smooth, dashed line) for a value of  $T$  that gave the minimum  $\chi^2$  for the preferred value of  $N(\text{D I})$  in Table 2. This is a smoothed version of the N I profile (heavy, solid line) that was obtained from the convolution by the kernel  $\phi_D(7m_p/3, T, v)$  from Eq. 3.

In addition to allowing  $T$  to vary, we also allowed for the existence of a uniform velocity offset between N I and D I, in recognition of the possibility that either our wavelength scale or the laboratory wavelengths of the N I features had some small, systematic errors.

#### 4.2. Allowances for Random and Systematic Errors

The presence of random errors due to noise fluctuations in the signal presents the usual challenge of determining the most probable result for  $N(\text{D I})$  and permissible variations that still give an acceptable fit to the data. On top of this we must consider additional uncertainties caused by systematic errors. The ones that we can identify easily are the inaccuracies in defining the background level for both lines (§3.3) and the contamination signal in the  $\text{L}\delta$  profile (§3.2). Additional parameters that could affect the outcome are the temperature of the gas  $T$  through its effect in making the deuterium profile smoother than the N I template (§4.1), the difference in the zero points of the N I and D I velocity scales, and the adopted heights and slopes of the continuum levels over the deuterium  $\text{L}\delta$  and  $\text{L}\epsilon$  absorption features. Our tactic for coping with these systematic errors was to express them in terms of simple parameters that could vary and then consider them in a unified analysis. Since these errors could be correlated, we felt that it would be unwise to analyze them separately.

We determined how well the data conform to various combinations of parameter values by evaluating the conventional  $\chi^2$  statistic,  $\sum[(I_{\text{meas}} - I_{\text{exp}})/\sigma_I]^2$ , where  $I_{\text{meas}}$  is a measured intensity with uncertainty  $\sigma_I$ , and  $I_{\text{exp}}$  is the expected intensity given the specified set of parameter values. Useful discussions of how to interpret the determinations of  $\chi^2$  when there are many free parameters are given by Lampton, et al. (1976) and Bevington & Robinson (1992, p. 212). The basic scheme is to find the minimum value  $\chi^2(\text{min})$  that arises when all parameters that influence  $I_{\text{exp}}$  are free to vary, and then examine the deviations  $\chi^2 - \chi^2(\text{min})$  as the parameters stray from their optimum values. Our  $\chi^2$  values represented a sum over both the  $\text{L}\delta$  and  $\text{L}\epsilon$  features taken together. This approach is similar to one adopted by Burles & Tytler (1998a) in their analysis of the deuterium abundance in a quasar absorption line system, except that we decouple the hydrogen measurements (§5) from those of deuterium because they are fundamentally different from each other.

To limit the number of degrees of freedom that apply to the confidence intervals for the outcomes that we are interested in, we segregated the free parameters into two fundamental categories. First, we recognized those parameters that had an astrophysical significance,  $N(\text{D I})$  and  $T$ . We sought to find a confidence interval that constrained these two parameters simultaneously. While  $T$  might seem to be an incidental parameter outside the objective of this study, there were good physical reasons for our verifying that no appreciable portion of the probability density wandered above or below acceptable limits. The second category contained parameters that were of no particular interest to us, i.e., nuisance parameters, but ones that had to be allowed to change freely as we re-minimized the  $\chi^2$  for every new trial combination of  $N(\text{D I})$  and  $T$ . We had no profound reason to require that any of these variables in the second category be constrained, and thus we could consider a projection of the lowest  $\chi^2$  values in the multi-dimensional space of these variables onto just the  $N(\text{D I})$ – $T$  plane. This allowed us to restrict the number of the degrees of freedom (df) that applied to the confidence intervals down to only 2.

In summary, parameters that mattered were (1)  $N(\text{D I})$  and (2)  $T$ , while those that did not were (3) the coefficient  $R_c$  for scaling the contamination signal (§3.2), (4) a relative velocity error  $\Delta v_{\text{N,D}}$  between the N I profile template (§4.1) and the deuterium absorption, (5 and 6) the background levels in the bottom of the H  $\text{L}\delta$  and  $\text{L}\epsilon$  features, and finally (7 through 10) the two coefficients that described the continuum straight lines spanning the D  $\text{L}\delta$  and  $\text{L}\epsilon$  features, i.e., in each case the level near the middle of the D feature and the slope of the line.<sup>9</sup>

---

<sup>9</sup>While one might argue that the continuum is not straight and has a curvature produced by the damping wings of the H I absorption, this effect is probably small enough to be masked by a curvature in the opposite direction caused by the broad stellar hydrogen feature. For the value of  $N(\text{H I})$  given in §5, the damping



### 4.3. Determination of $N(\text{D I})$ and its Uncertainty

From our knowledge of the CCD readout noise and dark current combined with the statistical fluctuations in the (background + signal) photons, we made an initial estimate for the uncertainties in the individual measurements of intensity  $\sigma_I$  at each velocity. We determined the correlation length for these errors by comparing fluctuations of intensity at a velocity  $v$  with those of  $v + \Delta v$ . The correlations disappear for  $\Delta v = 1.25 \text{ km s}^{-1}$ , which is exactly the width of each pixel in the CCD.<sup>10</sup> Our determinations of  $\chi^2$  discussed below relied on intensities separated by this value for  $\Delta v$ .

The most important terms in the summation for  $\chi^2$  are those that are directly influenced by trial values of  $N(\text{D I})$  and  $T$ , through differences over the (deuterium line) velocity interval  $-10$  to  $+40 \text{ km s}^{-1}$  between measured intensities  $I_{\text{meas}}$  and the computed values of  $I_{\text{exp}}$ , the expected absorption profile multiplied by a local continuum level. At the same time, parameters that define the continuum contribute to  $\chi^2$  through the deviations between  $I_{\text{meas}}$  and straight-line extrapolations over the intervals  $(-100$  to  $-10, +40$  to  $+47 \text{ km s}^{-1})$  for  $\text{L}\delta$  and  $(-55$  to  $-10, +40$  to  $+50 \text{ km s}^{-1})$  for  $\text{L}\epsilon$  (see Fig 3). Likewise,  $\chi^2$  is influenced by modifications in the background zero level that must be subtracted from the raw intensities at all velocities: we allowed the sum to include deviations away from zero for the background-corrected fluxes over the heavily saturated portion of the H profile from  $+60$  to  $+140 \text{ km s}^{-1}$  (for the D line heliocentric velocity scales shown in Figs. 1 and 3). Finally, fluxes over all velocities in the  $\text{L}\delta$  profile can be modified by the contamination correction signal, whose amplitude was allowed to vary as we searched for a minimum  $\chi^2$  in each case.

We had a total of 320 independent intensity measurements to constrain the 10 free parameters listed at the end of §4.2, so we should insist that the minimum  $\chi^2$  agree with a reasonable expectation for  $\text{df} = 310$ . In fact, with our original estimate for the noise in the measurements, we arrived at a minimum  $\chi^2 = 225$ , a value that was unreasonably low. In later calculations, we rescaled this noise level by a factor  $\sqrt{225/278} = 0.90$ , since we had

---

wing absorbs only 9% of the flux at the D  $\text{L}\delta$  line and 2% at the D  $\text{L}\epsilon$  line. Moreover, the *appearance* of the continuum suggests that a straight-line fit is justified – see Fig. 3.

<sup>10</sup>This is not a trivial finding. In an electron-bombarded CCD image sensor, correlation lengths greater than a CCD pixel can result if the diameter of the secondary electron cloud from each event is of order or larger than a CCD pixel (Jenkins et al. 1988). Events straddling a pixel boundary, for instance, will create a correlated signal in both pixels that pick up the secondary charges. Evidently such events are not common enough to cause a statistically significant effect, otherwise we would have found correlation lengths greater than  $1.25 \text{ km s}^{-1}$ .

a 90% confidence that the minimum  $\chi^2$  should be at least equal to 278 for  $\text{df} = 310$ . We felt that it was legitimate for us to perform a *post facto* rescaling of the noise, because our original estimate was accurate to only a level of about 25%. This rescaling is a conservative one, because it's more probable that the minimum  $\chi^2$  should really be about equal to 310. If we had used 310 instead of 278 in the expression for the noise multiplication factor, we accordingly would have found tighter limits for  $N(\text{D I})$  because the  $\chi^2$  expressions would have increased more rapidly as we deviated away from the most probable  $N(\text{D I})$ .

To find the minimum  $\chi^2$ , we used Powell's method of converging to the minimum of a multi-dimensional function (Press et al. 1992, p. 406). After finding this minimum and noting the most probable  $N(\text{D I})$ , we then evaluated the confidence interval for  $N(\text{D I})$  by forcing this parameter to vary, but at the same time allowing the other 9 parameters to adjust to new minima in  $\chi^2$ . Our target values for the new minima corresponded to  $\chi^2(\text{min}) + 4.6$  and  $\chi^2(\text{min}) + 9.2$  for the 90% and 99% confidence limits (i.e., “1.65 $\sigma$ ” and “2.58 $\sigma$ ” deviations), respectively, where  $\chi^2(\text{min})$  is the overall minimum at the preferred value of  $N(\text{D I})$  as shown in Table 2. This exercise ultimately led to the limiting values for  $N(\text{D I})$  listed in the table. Over the full range of  $N(\text{D I})$  between the most extreme limits, the temperature  $T$  was the only parameter that showed any profound change. For this reason,  $T$  is also listed. Our result for the most probable  $N(\text{D I})$  is in near perfect agreement with the value  $\log N(\text{D I}) = 15.08$  reported by Laurent, et al (1979) in their investigation that led to a value  $\text{D}/\text{H} = 7 \times 10^{-6}$  using data from *Copernicus*.

Fig. 3 shows the observed deuterium profiles along with the expected absorption profiles (upper and lower boundaries of the crosshatched regions) whose shapes are determined by the shape of the  $\text{N I}$  profile (heavy, solid line in Fig. 2) after it has been smoothed to allow for possible extra thermal Doppler motions that would be expected for the lighter atoms (dashed line in Fig. 2). Basically, apart from the thermal smearing, there is no evidence that there are deviations between the nitrogen and deuterium velocity profiles.

In Fig. 3 we also illustrate with a dashed line the depth and shape of the expected profile if  $N(\text{D I})$  were as high as  $2.34 \times 10^{15} \text{cm}^{-2}$ , a value that would give  $\text{D}/\text{H} = 1.5 \times 10^{-5}$  as seen elsewhere (§2) if  $N(\text{H I}) = 1.56 \times 10^{20} \text{cm}^{-2}$  (§5 below). When  $N(\text{D I})$  is forced to this large value,  $\chi^2_{\text{min}}$  occurs at  $T \leq 300\text{K}$ . This value seems unrealistically low, in view of the evidence that the 0–1 rotational temperature of  $\text{H}_2$  toward  $\delta$  Ori A is 1625 K (Savage et al. 1977). Thus, we set a constraint  $T = 1625\text{K}$  (but allowed other free parameters to float) when we constructed the dashed line in Fig. 3. For this case,  $\chi^2 - \chi^2_{\text{min}} = 36.3$  which is clearly unacceptable.

Table 2. Limits for  $N(\text{D I})$  from the  $\chi^2$  Analysis

Significance	$N(\text{D I})$ ( $10^{15}\text{cm}^{-2}$ )	$T^a$ (K)	$\chi^2$
Minimum $N(\text{D I})$ at the 99% confidence limit	0.89	6800	286.1
Minimum $N(\text{D I})$ at the 90% confidence limit	0.96	6600	281.7
Best $N(\text{D I})$ .....	1.16	5900	277.0
Maximum $N(\text{D I})$ at the 90% confidence limit	1.45	3500	281.7
Maximum $N(\text{D I})$ at the 99% confidence limit	1.61	2400	286.2

<sup>a</sup>The 99% confidence limits for  $T$  if the value of  $N(\text{D I})$  is allowed to float is 1000 K [at  $N(\text{D I}) = 1.41 \times 10^{15}\text{cm}^{-2}$ ] and 14,500 K [at  $N(\text{D I}) = 1.12 \times 10^{15}\text{cm}^{-2}$ ]. [The 90% limits are (2200 K,  $1.30 \times 10^{15}\text{cm}^{-2}$ ) and (11,000 K,  $1.12 \times 10^{15}\text{cm}^{-2}$ ).] This indicates that we are not including physically implausible temperatures in the simultaneously permitted combinations for the two parameters  $N(\text{D I})$  and  $T$ . It also reveals that extreme deviations in  $T$  have only a mild effect on our answer for  $N(\text{D I})$ , which is a good justification for our simplifying assumption that  $T$  does not vary between superposed velocity components.

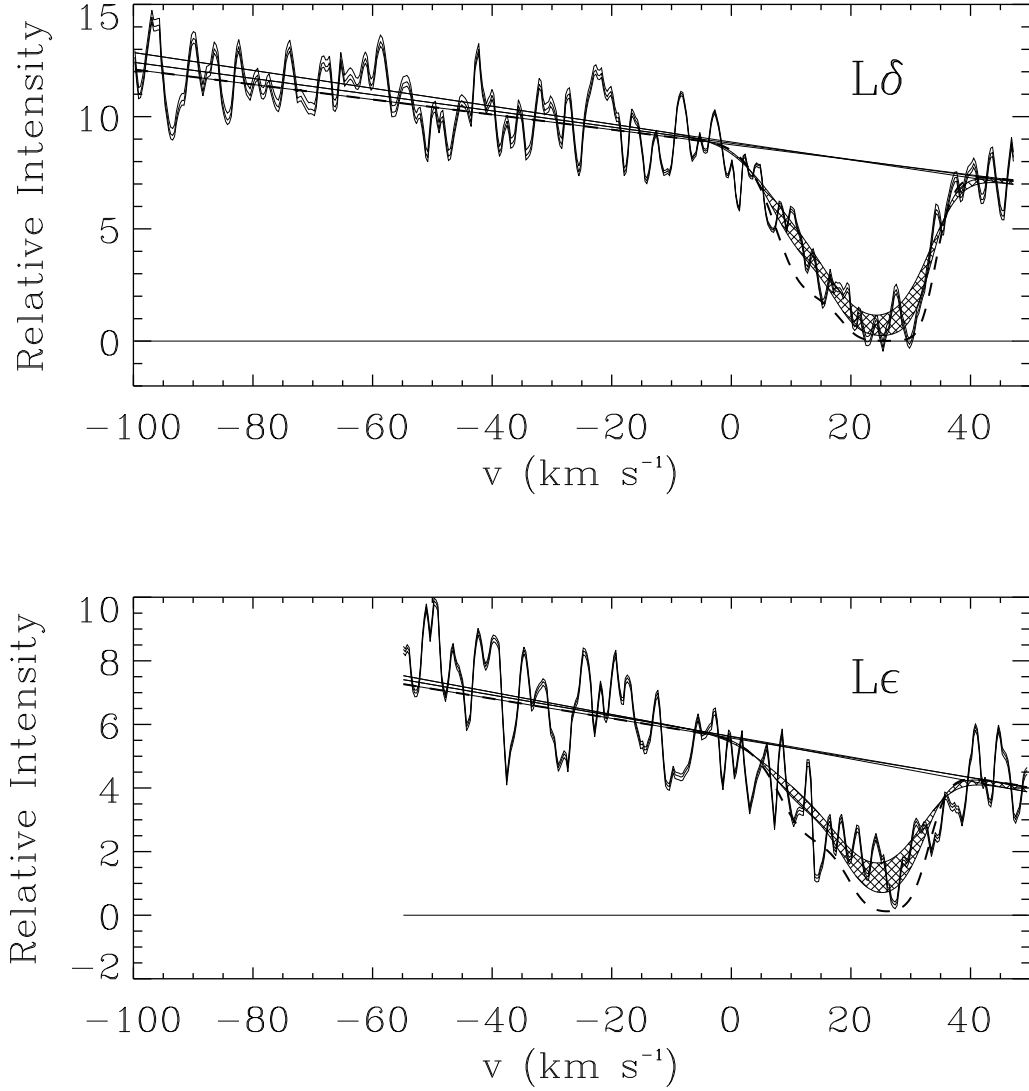


Fig. 3.— Regions containing acceptable model deuterium  $L\delta$  and  $L\epsilon$  profiles (crosshatched zones), bounded by the computed profiles that correspond to the lower and upper bounds of the 90% confidence interval for  $N(\text{D I})$  given in Table 2 (smooth, solid curves), plotted on top of the actual data. Very small changes in the continuum levels sought by the  $\chi^2$  minimizations are also shown for the limiting values [in both cases, the lower  $N(\text{D I})$  seeks a continuum with a more negative slope]. Very small differences in the favored values of the free parameters (3) through (6) identified at the end of §4.2 lead to small differences in the adjusted fluxes. Dashed lines show the profiles that would be expected if  $N(\text{D I}) = 2.34 \times 10^{15} \text{ cm}^{-2}$ , a value that would be consistent with  $\text{D}/\text{H} = 1.5 \times 10^{-5}$  measured for the local interstellar medium in front of  $\alpha$  Aur (Linsky et al. 1995) and HR1099 (Piskunov et al. 1997).

## 5. A Redetermination of $N(\text{H I})$

Published values of  $N(\text{H I})$  based on moderate resolution recordings of the  $\text{L}\alpha$  absorption in the spectrum of  $\delta$  Ori range from  $1.25_{-0.28}^{+0.33} \times 10^{20} \text{ cm}^{-2}$  (Jenkins 1970), based on photographic spectra recorded on sounding rocket flights, to  $1.7 \pm 0.34 \times 10^{20} \text{ cm}^{-2}$  (Bohlin, Savage, & Drake 1978) from a spectrum recorded by *Copernicus*. Since  $\delta$  Ori is a hot star (O9.5II), the stellar H I absorption line makes a negligible contribution to  $N(\text{H I})$ .<sup>11</sup> The accuracies of these measurements are satisfactory for studies of general trends, but for measuring D/H, and in particular to investigate the possible spatial variability of D/H, we must strive for a precision in  $N(\text{H I})$  that is as good as or preferably better than that for  $N(\text{D I})$ .

The H absorption features shown in Fig. 1 are of no use in determining  $N(\text{H I})$  because the lines are heavily saturated, and most of the absorption is by small amounts of hydrogen with velocities well displaced from the line core. The damping wings of these lines are too weak to measure. In contrast, the  $\text{L}\alpha$  feature has very strong wings, ones that make this feature the least susceptible of all the Lyman series lines to any contributions from high-velocity wisps of H I that do not produce detectable counterparts in D I absorption. It is for this reason that we concluded that the  $\text{L}\alpha$  feature was the best indicator of  $N(\text{H I})$ .

Spectra of  $\delta$  Ori obtained with the *International Ultraviolet Explorer* (IUE) in high-dispersion mode (FWHM  $\approx 25 \text{ km s}^{-1}$ ) were particularly attractive for our study of the  $\text{L}\alpha$  feature for several reasons. First, the alternative was to use archival *Copernicus* data ( $\text{L}\alpha$  was not recorded by IMAPS or HST), but the only available *Copernicus* data with sufficiently broad wavelength coverage of  $\text{L}\alpha$  were obtained with the low-resolution U2 detector, and for this detector uncertainties are introduced by stray light from the vent hole (Rogerson et al. 1973), an effect that requires a special correction (Bohlin 1975) of uncertain accuracy. Second, a large number of observations of  $\delta$  Ori obtained under slightly different observing conditions (e.g., small aperture *vs.* large aperture) over the course of many years are available from the IUE archive. By analyzing all of the IUE exposures rather than a single observation, we can validate our estimates of random errors and also increase our chances of exposing *systematic* errors in the derivation of  $N(\text{H I})$ . Finally, our ability to combine many observations allowed us to reduce the effects from random noise by brute force.

A potentially important source of systematic error is the fact that  $\delta$  Ori is a complex

---

<sup>11</sup>Diplas & Savage (1994) have estimated that the equivalent H I column density caused by stellar absorption for  $\delta$  Ori is  $10^{17.6} \text{ cm}^{-2}$ . Therefore correcting for the stellar  $\text{L}\alpha$  line changes  $\log N(\text{H I})$  by only 0.01 dex.

multiple-star system. The primary (component A) is a single-lined spectroscopic binary that is important in the history of ISM research: stationary Ca II absorption features in its spectrum provided the earliest evidence of interstellar gas (Hartmann 1904). The velocity amplitude of the binary is  $98 \text{ km s}^{-1}$ , and it has a period of 5.7 days (Harvey et al. 1987). It is also a partially eclipsing binary (Koch & Hrivnak 1981), and it has a visual companion of comparable brightness at a separation of  $\sim 0''.2$  (Heintz 1980; McAlister & Hendry 1982). The spectroscopic binary nature of the star system presents an opportunity to investigate systematic errors in the determination of the interstellar  $N(\text{H I})$ : the H I  $\text{L}\alpha$  profile is extremely broad, and if there are unrecognized stellar lines in the principal part of the Lorentz wings of the  $\text{L}\alpha$  feature, then their additional optical depth could lead to an overestimate of  $N(\text{H I})$ . However, such stellar lines should move in velocity as the binary traverses its orbit, and this may lead to different values of  $N(\text{H I})$  when observations made at different times are analyzed. If this occurs, then we should see  $N(\text{H I})$  change as a function of the spectroscopic binary phase. Similarly, we can check for systematic changes in  $N(\text{H I})$  when the multiple star enters the partial eclipses over the phase intervals 0.9–0.1 and 0.4–0.6. While any dependence on phase may uncover an influence that stellar features have on the outcome, there is no guarantee that they do not perturb our result in a manner that is uniform over all phases.

According to the NSSDC archive, there are 59 IUE observations of  $\delta$  Ori obtained with the Short Wavelength Prime (SWP) camera in the high-dispersion echelle mode. We screened these observations for saturated exposures, missing data, or other problems and rejected two of the observations, leaving 57 spectra for our analysis. Using the standard IUE RDAF software, we selected the spectral regions of interest from the standard IUESIPS data rather than the NEWSIPS reductions since there are a number of problems with NEWSIPS processing as applied to high dispersion spectra that could adversely affect our analysis (Massa et al. 1998).

In the vicinity of the  $\text{L}\alpha$  line the orders on the IUE detector are closely spaced, and scattered light from adjacent orders overlaps in the interorder region causing an incorrect background subtraction and zero intensity level when using the standard software. We used the method of Bianchi & Bohlin (1984) to correct for this problem. Also, in some cases, a velocity shift was applied to the IUE data based on the position of the N I triplet at  $1200 \text{ \AA}$  compared to that expected from the IMAPS N I profile (§4.1) with optical depths rescaled to account for the stronger transition probabilities. This should register all of the IUE data to the correct velocity scale to an accuracy of better than  $\pm 5 \text{ km s}^{-1}$ , which is more than adequate for a determination of  $N(\text{H I})$  since we are fitting *both* of the strong damping wings of the  $\text{L}\alpha$  profile (an error of  $5 \text{ km s}^{-1}$  in the velocity scale zero point changes  $N(\text{H I})$  by an insignificant amount).

IUE data contain a number of perturbations in addition to the usual photon counting noise. They show strong fixed pattern noise, “hot spots” which mimic emission features, and drop-outs where the reseaux used to correct for camera distortions happen to fall on the spectrum (Harris & Sonneborn 1987). In addition, the spectra occasionally show artifacts at the transitions between echelle orders due to errors in the ripple correction (see below). Again, by analyzing *all* of the IUE data, we can reduce the impact of these noise sources, which are present in some of the observations and are not apparent in others. We ascertained that there was no *persistent* nonlinearity in the photometric response of IUE by comparing its  $L\alpha$  profiles of HD 93521 and HD 74455 with those recorded for the same stars by the GHRS on HST with the medium-resolution grating (G160M). Departures from the GHRS spectra near the breaks in the IUE echelle orders seem to come and go, but aside from the greater random noise in the IUE spectra, the spectra are usually very similar to each other.

In simplest terms, our means for constraining the H I column density followed a method introduced by Jenkins (1971) and used later by Bohlin (1975), Bohlin, et al (1978), Shull & van Steenberg (1985), and Diplas & Savage (1994): we determined the  $N(\text{H I})$  that provides the best fit to the  $L\alpha$  profile with the optical depth  $\tau$  at a given wavelength  $\lambda$  calculated from the expression

$$\tau(\lambda) = N(\text{H I})\sigma(\lambda) = 4.26 \times 10^{-20} N(\text{H I})(\lambda - \lambda_0)^{-2} \quad (4)$$

(Jenkins 1971), where  $\lambda_0$  is the  $L\alpha$  line center at the velocity centroid of the hydrogen. However, we went a step further by employing the technique used to estimate  $N(\text{D I})$  in §4.3, i.e., we first determined the important free parameters that could be adjusted to fit the H I  $L\alpha$  absorption profile, then we found the set of parameters that minimized  $\chi^2$  using Powell’s method, and finally we set confidence limits on the H I column density by increasing (or decreasing)  $N(\text{H I})$  with the other parameters freely varying until  $\chi^2$  increased by the appropriate amount for the confidence limit of interest.

Figure 4 shows a sample IUE spectrum in the vicinity of the  $L\alpha$  absorption line. From this figure one can see that the continuum is close to linear in this region. However, it is possible that the continuum has a slight downward or upward curvature, so we assumed a second-order polynomial to describe the continuum and allowed the  $\chi^2$  minimization process to determine the continuum shape that provided the best fit to the  $L\alpha$  profile. Therefore the free parameters for fitting the H I profile were  $N(\text{H I})$ , three coefficients that specify the second-order continuum polynomial, and a simple additive correction to the intensity zero point.<sup>12</sup>

---

<sup>12</sup>Despite our use of the Bianchi & Bohlin (1984) correction, in many cases inspection of the flat-bottomed,

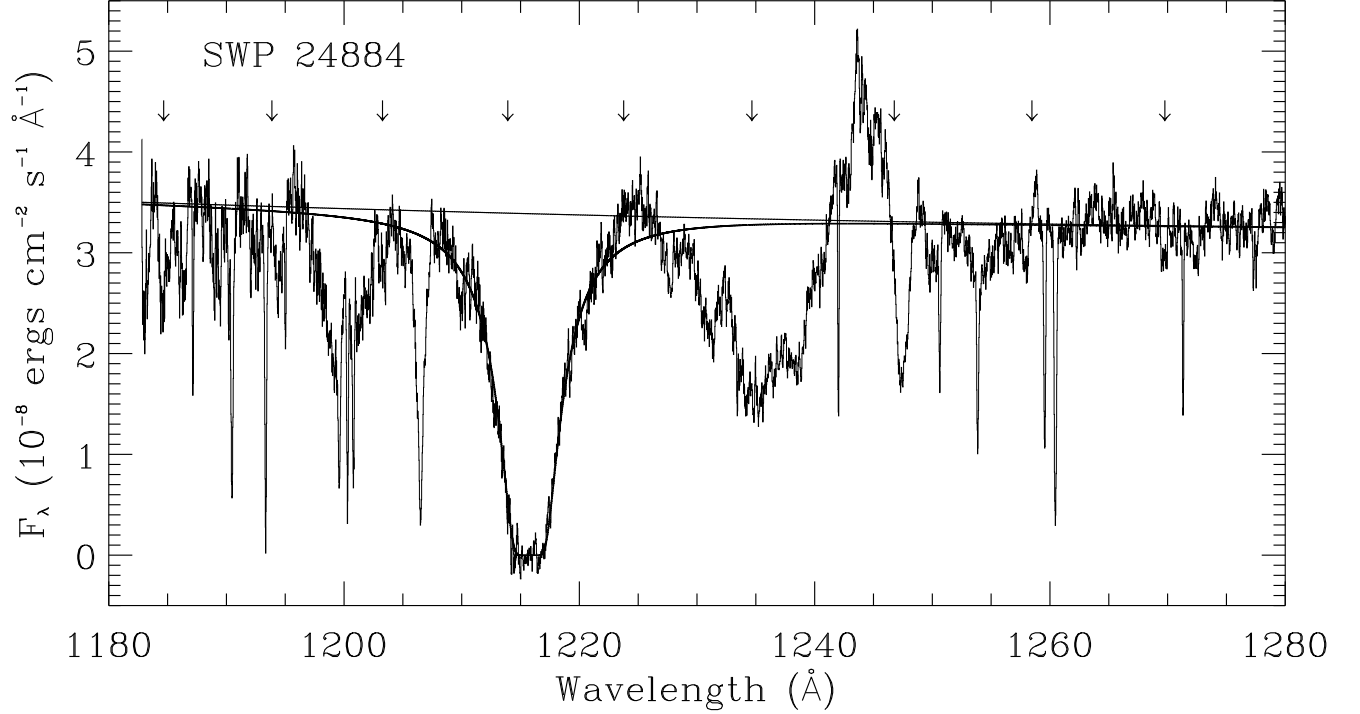


Fig. 4.— A sample high-dispersion spectrum of  $\delta$  Ori A in the vicinity of  $L\alpha$  showing the second-order polynomial fitted to the continuum and the computed profile for the preferred value of  $N(\text{H I})$ . This IUE spectrum has been smoothed with a 5-pixel boxcar for display purposes only; the unsmoothed data were used to constrain  $N(\text{H I})$  as described in the text. Due to the presence of the N V P-Cygni profile longward of  $L\alpha$  and several strong lines (e.g., Si III  $\lambda 1206.5$ ) shortward, the continuum fitting regions are somewhat far-removed from the  $L\alpha$  region. Nevertheless, the continuum is well constrained. The transitions between orders are indicated with arrows. Small artifacts are occasionally present at some order transitions due to errors in the ripple correction.



We point out that the continuum placement is constrained not only by the fits to regions that are far removed from the  $L\alpha$  feature, but also by requiring a good match to the shapes of its damping wings. For instance, if the continuum is badly placed or has too much upward or downward curvature, then a poor fit results. In particular, if we artificially forced the continuum to have a downward curvature (in an experimental challenge to lower  $N(\text{H I})$  and thus provide a higher  $D(\text{H})$ ), we obtained clearly inferior fits. We found that in the course of our minimizing  $\chi^2$  that we could always simultaneously obtain a good fit to the profile and match the outlying fluxes with a nearly flat continuum.

Figure 5 shows two examples of H I  $L\alpha$  profiles observed with IUE, along with the computed profiles for the lower and upper bounds on  $N(\text{H I})$  at the 90% confidence level for each case. The final continua corresponding to the upper and lower bounds are plotted with dashed lines. Panel (a) shows a typical spectrum, while (b) shows examples of artifacts at  $\lambda \sim 1214.4$  and  $1224.8 \text{ \AA}$  that we encountered at the transitions between IUE echelle orders. Assuming these to be artifacts due to the ripple correction, we used only the sides of the  $L\alpha$  profile in the wavelength ranges  $1209.0\text{--}1213.5 \text{ \AA}$  and  $1217.14\text{--}1223.0 \text{ \AA}$  and thereby excluded these artifacts from the  $\chi^2$  calculation. This procedure resulted in bounding profiles such as those shown in both of the panels of the Figure. However, as an experiment we also processed all of the IUE data including the region at  $\sim 1214.4 \text{ \AA}$  in the  $\chi^2$  calculation in order to evaluate the importance of this effect on the final results (see below).

It is important to note that the great strength of the  $L\alpha$  profile makes the Lorentzian wings dominate over the effects of instrumental or Doppler broadening. Gas that is known to exist in the vicinity of the Orion association at high velocities ( $v \approx -100 \text{ km s}^{-1}$ ) (Cowie, Songaila, & York 1979) should not be important, since the absorptions from any wisps of H I at such velocities are displaced by only about  $0.3 \text{ \AA}$  relative to the line center.

Figure 6 shows the logarithms of the derived H I column densities with their  $1\sigma$  error bars, plotted as a function of the spectroscopic binary phase, for all of the IUE SWP data except the two rejected exposures. We calculated the phase using the period and  $T_0$  derived by Harvey, et al. (1987) from their analysis of all suitable data from 1902–1982 (including some of the IUE data used here). There are no obvious systematic trends as function of spectroscopic binary phase evident in this plot, which gives us some assurance that weak stellar lines do not significantly affect the derived  $N(\text{H I})$ . In the figure, large and small

---

saturated portion of the  $L\alpha$  profile showed that the zero intensity level was not quite correct, so we included a zero point shift as a free parameter and used intensity points within the saturated core as one of the collections of terms for calculating  $\chi^2$ .

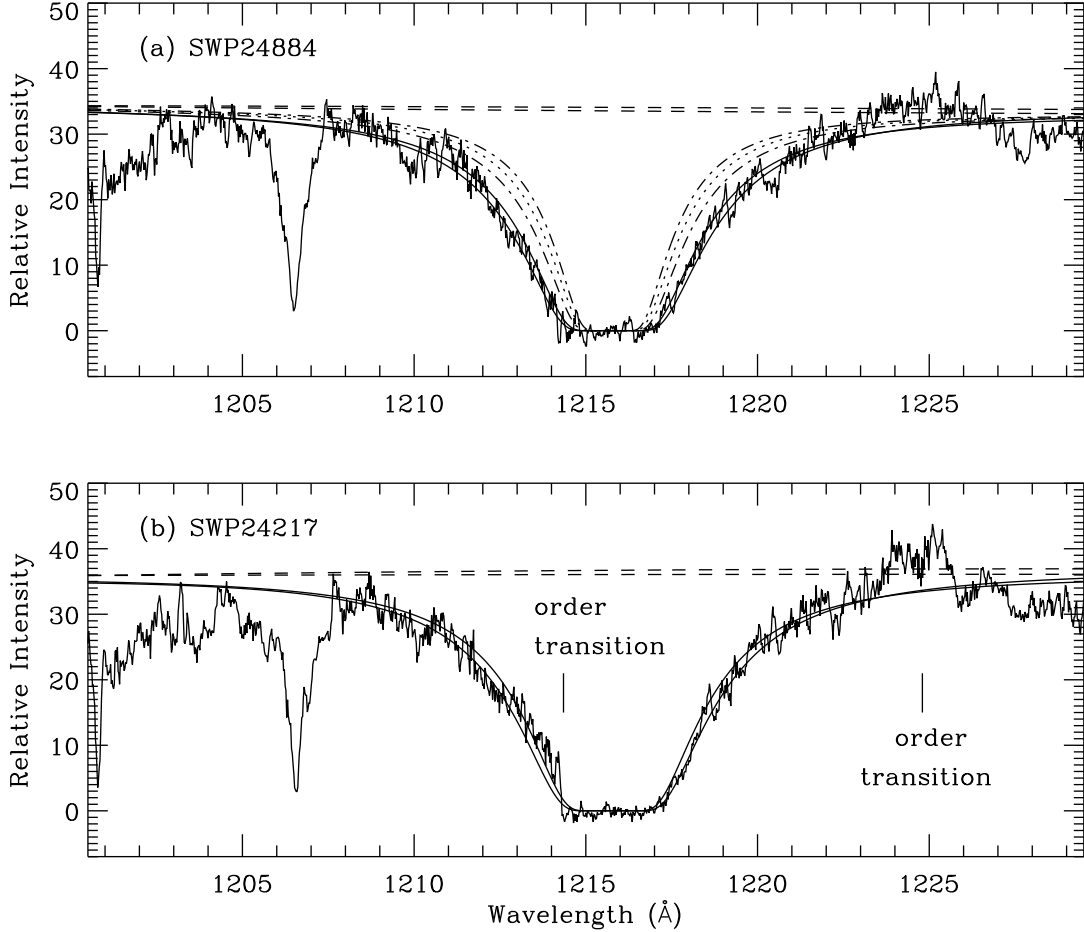


Fig. 5.— Examples of high-dispersion IUE spectra of the H I  $L\alpha$  line in the spectrum of  $\delta$  Ori A. Panel (a) shows a normal IUE spectrum while (b) shows a spectrum with the peculiar features at the order transitions near 1214.4 and 1224.8 Å. Computed profiles for the upper and lower bounds on  $N(\text{H I})$  at the 90% confidence levels for the individual cases are overplotted on the IUE data, and the continua corresponding to these upper and lower bounds are shown with dashed lines. The narrower damping profiles well inside the observed profile in the upper panel indicate the expected appearance if  $D/H$  were equal to the more general result  $1.5 \times 10^{-5}$  discussed in §2 with our values of  $N(\text{D I})$  given in Table 2 (dotted line = most probable value, dot-dashed line = 90% confidence limits). The IUE spectra have been smoothed with a 5-pixel boxcar for display purposes only; the unsmoothed data were used to constrain  $N(\text{H I})$  as described in the text.

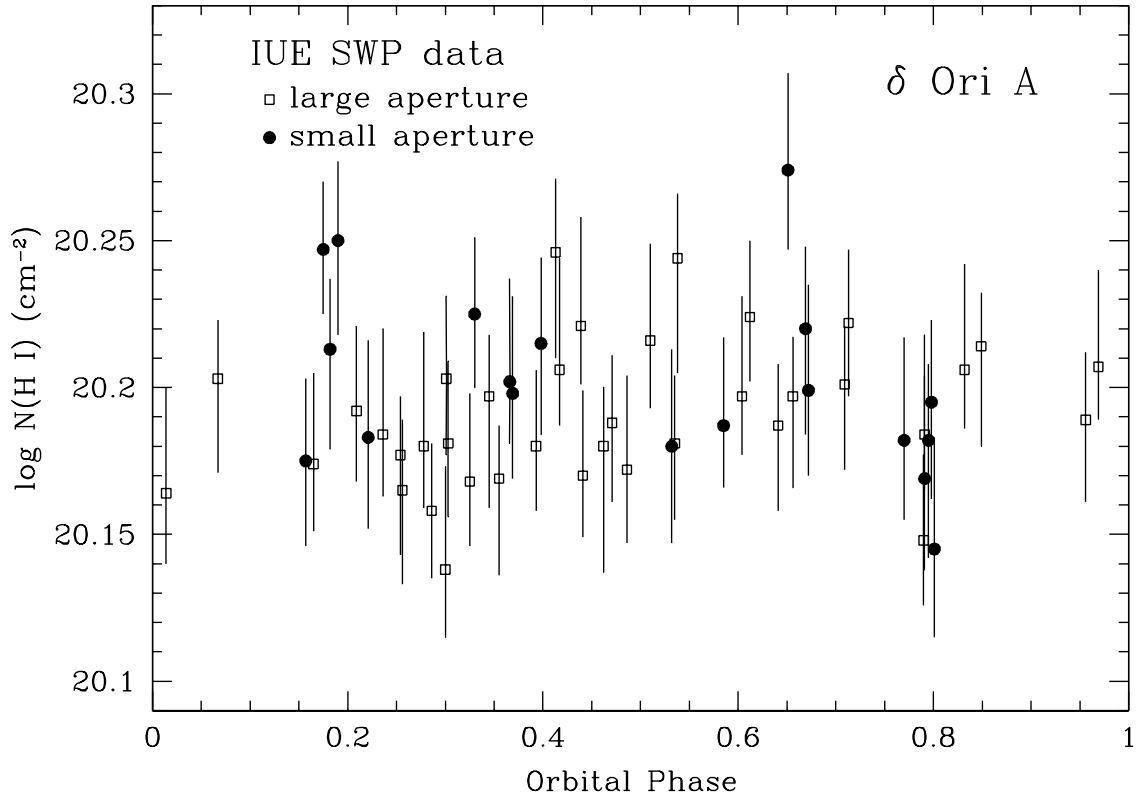


Fig. 6.— H I column densities toward  $\delta$  Ori A derived from 57 IUE observations as described in the text, plotted versus phase of the spectroscopic binary. Each column density is plotted with  $\pm 1\sigma$  error bars. Large aperture data are shown with open squares while small aperture data are indicated with filled circles.

aperture data are shown with different symbols to check for any systematic differences, and no differences are readily apparent. With only the large aperture data we derive a mean H I column density of  $\langle N(\text{H I}) \rangle = 1.54 \times 10^{20} \text{ cm}^{-2}$  with an rms dispersion  $\sigma = 0.08 \times 10^{20}$  [both quantities are weighted inversely by the variances of the individual  $N(\text{H I})$  estimates]. With the small aperture data, we obtain  $\langle N(\text{H I}) \rangle = 1.59 \times 10^{20} \text{ cm}^{-2}$  with  $\sigma = 0.11 \times 10^{20}$ . Therefore it appears appropriate to combine the large and small aperture data to constrain  $N(\text{H I})$ . Using the entire IUE data set, we obtain  $\langle N(\text{H I}) \rangle = 1.56 \times 10^{20} \text{ cm}^{-2}$  with an rms scatter equal to  $0.09 \times 10^{20}$ . Since there are 57 measurements, the error in the mean  $= \sigma/\sqrt{57} = 0.01 \times 10^{20}$  for the whole data set. We find that including the region that spans the ripple correction artifact at  $1214.4 \text{ \AA}$  shown in Figure 5(b) lowers the overall result by less than 0.01 dex. This is because the feature is present in only a small fraction of the IUE spectra.

The scatter in Figure 6 appears to be due entirely to the uncertainties from noise in the individual measurements: the value for  $\chi^2 = \sum_i \{[N_i(\text{H I}) - \langle N(\text{H I}) \rangle] / \sigma [N(\text{H I})]_i\}^2$  calculated for the entire data set is 50.32, which implies a reduced  $\chi^2$ ,  $\chi^2/56 = 0.90$ . *Nevertheless, given the many potential sources of systematic error in these particular IUE data, it is still possible that there are some unrecognized systematic errors which affect  $N(\text{H I})$  and that the real error in the mean is underestimated.* However, the good fits to the H I  $\text{L}\alpha$  profiles (see Fig. 5) and the lack of pronounced variations with binary phase indicate that such unrecognized systematics are not likely to be large.<sup>13</sup> It is reassuring to note that a constant, systematic error in the result for  $N(\text{H I})$  would need to be at least 15 times as large as the formal (random) error before it could have a meaningful effect on the overall error for D/H derived in §6 below. In the light of our deliberate attempt to uncover such systematic errors in the study of  $N(\text{H I})$  vs. orbital phase, we are confident that they could not have such a large numerical advantage, which means they are unlikely to be a critical issue in this investigation.

Finally, to illustrate more graphically our confidence in the H I result, we show with dotted and dash-dot damping profiles in Fig. 5(a) the expected appearance of the  $\text{L}\alpha$  absorption if our  $N(\text{D I})$  derivations are correct but  $N(\text{H I})$  were low enough to make  $\text{D}/\text{H} = 1.5 \times 10^{-5}$ , as indicated for other lines of sight (§2). There seems to be no question

---

<sup>13</sup>In their study of an observation of  $\text{L}\alpha$  absorption in the spectrum  $\mu \text{ Col}$ , Howk, Savage and Fabian (1999) estimated a systematic error of 0.02 dex for a determination of  $N(\text{H I})$  somewhat less than  $10^{20} \text{ cm}^{-2}$ . This relative error is about half of the amount that would be needed to have any appreciable impact on the relative errors for our D/H toward  $\delta \text{ Ori A}$  given in §6. Although we must acknowledge that their GHRS spectrum is of much better quality than any that were taken by IUE, their independent estimate that gives a low value for the magnitude of a systematic error in this type of measurement is encouraging.

that the real data are strikingly inconsistent with these lower values for  $N(\text{H I})$ .

## 6. D/H toward $\delta$ Ori and its Significance

Combining the results reported in §4.3 and §5, we find that with 90% confidence we can declare that  $N(\text{D I})/N(\text{H I}) = 7.4_{-1.3}^{+1.9} \times 10^{-6}$  in the direction of  $\delta$  Ori A. The most noteworthy feature of this result is that it differs from most determinations of D/H along other lines of sight in our local region of the Galaxy (§2). It is clear that our value for D/H represents a deviation, even if one relies only on the HST observations that generally concentrate within the range  $\text{D/H} = 1.3 - 1.7 \times 10^{-5}$  in the very local medium and rejects the *Copernicus* results because their accuracies may have been overstated. Our result shows a simple velocity structure for the D I, N I and O I absorption profiles and thus removes the primary uncertainty that confronted Laurent, et al (1979). It also removes the grounds on which McCullough (1992) rejected the measurements of deuterium toward stars in Orion.

## 7. Abundances of Heavier Elements

Variations in the heavy element abundances of stars with similar ages, such as B stars in the Orion association (Cunha & Lambert 1994) or F and G type stars at a Galactocentric radius nearly the same as the Sun (Edvardsson et al. 1993), suggest that the ISM out of which the stars formed may be a heterogeneous mixture of gases with different levels of heavy element enrichment. This may possibly result from random dilutions of gas in the Galactic plane by metal-poor material falling in from the halo (Meyer et al. 1994). If the material in the direction of  $\delta$  Ori had a lower deuterium abundance because it had been subjected to more intensive stellar processing or less of this dilution, we would expect the heavy element abundances to be higher than elsewhere. For our test of this proposition, we will examine the abundances of oxygen and nitrogen, both of which are unlikely to be appreciably altered by depletions onto dust grains (Meyer, Cardelli, & Sofia 1997; Meyer, Jura, & Cardelli 1998). O I and N I are also good standards because their ionizations are closely coupled to that of H I (§4.1), and this allows us to neglect the higher stages of ionization because they should be identified only with ionized H and D. O and N are also useful for comparisons with abundance studies elsewhere in the Universe. These investigations are facilitated by the generous number of transitions in the ultraviolet with a broad range of  $f$  values (Timmes et al. 1997). [Argon is another element that is expected to have very little depletion, but it is not suitable for comparison because under many circumstances its ionization can differ appreciably from that of H (Sofia & Jenkins 1998).]

Meyer, et al. (1998) found from their measurement of the intersystem O I transition at 1356 Å that toward  $\delta$  Ori  $O/H = 2.82 \pm 0.46 \times 10^{-4}$  (from the same data that we used to construct the profile shown in Fig. 2). This value<sup>14</sup> is slightly less than their average of  $3.19 \pm 0.14 \times 10^{-4}$  over 13 lines of sight. Within the experimental errors, however, the value is consistent with the average. Meyer, et al. (1997) found that  $N/H = 7.5 \pm 0.4 \times 10^{-5}$  toward 6 stars. Since  $\delta$  Ori was not part of this sample, we must rely on our own measurement of N I which yields  $\int N_a(v)dv = 6.2 \times 10^{15} \text{cm}^{-2}$  – see §4.1 and the N I profile in Fig. 2. With our result for  $N(\text{H I})$ , we arrive at  $N/H = 4.0 \times 10^{-5}$ . Thus, we see no evidence that the gas has been specially enriched with material having a high abundance of heavy elements and, by virtue of a more intensive exposure to stellar interiors, a more thorough depletion of deuterium. In fact, the possible positive correspondence in the deviations in the N and D abundances is reminiscent of the suggested correlation (but with large errors) between D/H and Zn/H shown by York & Jura (1982). Of course, we must acknowledge that for nitrogen a comparison of our result for  $\delta$  Ori with the general measurements of Meyer, et al (1997) for other lines of sight may be compromised by errors in f values, since we used different transitions to determine  $N(\text{N I})$ .

## 8. Discussion

Our finding presented in §6 indicates that the most probable D/H toward  $\delta$  Ori is about half as large as that found from various HST investigations of the local ISM. Our result applies to an average over a range of velocities, which means that it represents a *lower limit* for the magnitude of deviations from the other cases. This anomaly is not linked with an increase in O/H or N/H, as one might expect from a simple explanation that a greater fraction of the gas had been cycled through stellar interiors. Of course, it may be possible to envision that the gas toward  $\delta$  Ori holds an unusually large fraction of material that has cycled only through the *outer envelopes* of stars, thus depleting the D without increasing the concentrations of heavier elements.

Recent observations of HD emission in the infrared from gas near Orion seem to confirm our finding that the abundance of deuterium is low in this region. Wright, et al. (1999) detected emission from the HD  $J = 1 \rightarrow 0$  transition at  $112 \mu\text{m}$  toward the Orion Bar with the Long Wavelength Spectrometer on board the *Infrared Space Observatory* (ISO). While there are some uncertainties in the rotation temperature of HD and the correction factors

---

<sup>14</sup>The value for  $N(\text{H I})$  adopted by Meyer, et al. (1998) was  $1.6 \times 10^{20} \text{cm}^{-2}$  which is very close to the result  $1.56 \times 10^{20} \text{cm}^{-2}$  that we derived in our more precise analysis (§5).

that must be applied to observations of the accompanying  $\text{H}_2$ , they arrived at a preferred value  $\text{HD}/\text{H}_2 = 2.0 \pm 0.6 \times 10^{-5}$  which leads to  $\text{D}/\text{H} = 1.0 \pm 0.3 \times 10^{-5}$  since there should be no appreciable D or H in atomic form. Their total range for D/H could be as large as 0.35 to  $1.30 \times 10^{-5}$  however. Bertoldi, et al. (1999) used the Short Wavelength Spectrometer on ISO and found a weak emission from the  $J = 6 \rightarrow 5$  transition at  $19.4 \mu\text{m}$  for HD in the Orion molecular outflow OMC-1. Again, corrections using information from models of the gas had to be made to interpret the results. Bertoldi, et al. (1999) concluded that  $\text{D}/\text{H} = 7.6 \pm 2.9 \times 10^{-6}$ . The measurements of HD by both groups seem to lead to results that are consistent with our determination of atomic D/H toward  $\delta$  Ori A.

Very distant gas systems that are registered in quasar absorption line spectra reveal apparent values of D/H that range from  $3 - 4 \times 10^{-5}$  (Burles & Tytler 1998a, b) to  $\sim 2 \times 10^{-4}$  (Songaila et al. 1994; Carswell et al. 1996; Rugers & Hogan 1996; Wampler et al. 1996; Webb et al. 1997; Tytler et al. 1999) – see reviews by Burles & Tytler (1998c) and Hogan (1998). The large dispersion in these outcomes might be attributable either to complications that arise from our incomplete knowledge of the chemical evolution of systems at large redshifts, the difficulty in obtaining accurate values of  $N(\text{H I})$ , or to the presence of random, weak, H I systems that masquerade as deuterium by having a velocity offset that is equal to about  $-80 \text{ km s}^{-1}$  from a main system. One might suppose that, in time, additional observations that include new cases or new data on existing ones may lead to a better understanding of the behavior of D/H in the Universe. Unfortunately, this optimistic belief may have been dealt a setback by our result that indicates that D/H could be driven by a process that we do not understand. Essentially, we see evidence that the ratio changes over a distance scale where the environment should be homogeneous, according to observations of other elements and generally accepted simple models for a galaxy’s chemical evolution and mixing rates in the ISM.

A few proposals to explain possible deviations in the balance of atomic D to H in the interstellar medium have been considered in the past. The simplest involves the selective incorporation of D into HD, an effect that can amplify  $\text{HD}/\text{H}_2$  to values well above the fundamental ratio of D to H (Watson 1973), but one that is probably counterbalanced by the more rapid photodissociation of HD in diffuse clouds because there is no self shielding (as there often is with  $\text{H}_2$ ). A preferential formation of HD is not responsible for the depletion of atomic D toward  $\delta$  Ori A, since  $\log N(\text{HD}) < 12.8$  (Spitzer, Cochran, & Hirshfeld 1974) (likewise, we see no HD features in our IMAPS spectrum). Another alternative, one advanced by Vidal-Madjar, et al. (1978) and Bruston et al. (1981), makes use of the differences in the ways that D and H can respond to radiation pressure, as a result of the very different opacities in the Lyman lines. They proposed that this effect could lead to a separation of the two species if there were a density gradient and a

nonisotropic radiation field. Finally, Jura (1982) has suggested that deuterium atoms could collide with dust grains, stick to them, and then be more strongly bound than hydrogen. Furthermore, he suggests that the mobility of the D atoms on the surfaces of these grains could be much lower than that of H, thus limiting the chances for combining with H atoms and being ejected as HD. One possible way to investigate the plausibility of this hypothesis might be to look for D–C or D–O stretch mode absorption features in dense clouds.

We look forward to the possibility that insights on the relationship for the variability in D/H to other interstellar parameters could arise from the anticipated large increase of information that should come from the *Far Ultraviolet Spectroscopic Explorer* (FUSE) after its launch in mid-1999. For the local ISM, the FUSE Principal Investigator Team has identified as potential targets<sup>15</sup> 7 cool stars, 19 white dwarfs, 9 late B- or early A-type stars, and 7 central stars of planetary nebulae for studying D/H in the first two years of operations.

The ORFEUS-SPAS project was a joint undertaking of the US and German space agencies, NASA and DARA. The successful execution of our observations was the product of efforts over many years by engineering teams at Princeton University Observatory, Ball Aerospace Systems Group (the industrial subcontractor for the IMAPS instrument) and Daimler-Benz Aerospace (the German firm that built the ASTRO-SPAS spacecraft and conducted mission operations). Contributions to the success of IMAPS also came from the generous efforts by many members of the Optics Branch of the NASA Goddard Space Flight Center (grating coatings and testing) and from O. H. W. Siegmund and S. R. Jelinsky at the Berkeley Space Sciences Laboratory (deposition of the photocathode material). This research was supported by NASA grants NAG5–616 to Princeton University and NAG5–3539 to Villanova University. We thank K. R. Sembach for supplying an IDL routine to apply the Bianchi & Bohlin correction to the IUE data. We also thank A. Vidal-Madjar, B. T. Draine and B. D. Savage for their helpful comments on early drafts of this paper. The O I absorption feature at 1355 Å was observed by the NASA/ESA Hubble Space Telescope. This spectral segment was obtained from the data archive at the Space Telescope Science Institute, operated by AURA under NASA contract NAS5-26555. The IUE data were obtained from the National Space Science Data Center (NSSDC) at NASA’s Goddard Space Flight Center.

---

<sup>15</sup>Details are given in the NASA Research Announcement for FUSE, dated Feb 9, 1998 (NRA 98-OSS-02), or else see <http://fusewww.gsfc.nasa.gov/fuse/>.



## REFERENCES

- Abgrall, H., & Roueff, E. 1989, A&AS, 79, 313
- Abgrall, H., Roueff, E., Launay, F., Roncin, J.-Y., & Subtil, J.-L. 1993a, A&AS, 101, 273
- 1993b, A&AS, 101, 323
- Bertoldi, F., Timmermann, R., Rosenthal, D., Drapatz, S. and Wright, C. M. 1999, A&A, submitted
- Bevington, P. R., & Robinson, D. K. 1992, Data Reduction and Error Analysis for the Physical Sciences, 2nd ed., (New York: McGraw Hill)
- Bianchi, L., & Bohlin, R. C. 1984, A&A, 134, 31
- Boesgaard, A. M., & Steigman, G. 1985, ARA&A, 23, 319
- Bohlin, R. C. 1975, ApJ, 200, 402
- Bohlin, R. C., Savage, B. D., & Drake, J. F. 1978, ApJ, 224, 132
- Bruston, P., Audouze, J., Vidal-Madjar, A., & Laurent, C. 1981, ApJ, 243, 161
- Burbidge, G., & Hoyle, F. 1998, ApJ, 509, L1
- Burles, S., & Tytler, D. 1998a, ApJ, 499, 699
- 1998b, ApJ, 507, 732
- 1998c, Space Sci. Rev., 84, 65
- Butler, S. E., & Dalgarno, A. 1979, ApJ, 234, 765
- Carswell, R. F., Webb, J. K., Lanzetta, K. M., Baldwin, J. A., Cooke, A. J., Williger, G. M., Rauch, M., Irwin, M. J., Robertson, J. G., & Shaver, P. A. 1996, MNRAS, 278, 506
- Cowie, L. L., Songaila, A., & York, D. G. 1979, ApJ, 230, 469
- Cunha, K., & Lambert, D. L. 1994, ApJ, 426, 170
- Dearborn, D. S. P., Steigman, G., & Tosi, M. 1996, ApJ, 465, 887
- Diplas, A., & Savage, B. D. 1994, ApJS, 93, 211
- Dring, A. R., Linsky, J., Murthy, J., Henry, R. C., Moos, W., Vidal-Madjar, A., Audouze, J., & Landsman, W. 1997, ApJ, 488, 760
- Edvardsson, B., Anderson, J., Gustafsson, B., Lambert, D. L., Nissen, P. E., & Tomkin, J. 1993, A&A, 275, 101
- Epstein, R. I., Lattimer, J. M., & Schramm, D. N. 1976, Nat, 263, 198

- Ferlet, R. 1981, *A&A*, 98, L1
- Field, G. B., & Steigman, G. 1971, *ApJ*, 166, 59
- Fitzpatrick, E. L. 1997, *ApJ*, 482, L199
- Gnedin, N. Y., & Ostriker, J. P. 1992, *ApJ*, 400, 1
- Gölz, M., Kappelman, N., Appenzeller, I., Barnstedt, J., Fromm, A., Grewing, M., Gringel, W., Haas, C., Hopfensitz, W., Krämer, G., Krautter, J., Lindenberger, A., Mandel, H., Werner, K., & Widmann, H. 1998, in *Proc. IAU Colloq. 166, The Local Bubble and Beyond*, ed. D. Breitschwerdt, M. J. Freyberg, & J. Trümper (Berlin: Springer), p. 75
- Goldbach, C., Lüdtke, T., Martin, M., & Nollez, G. 1992, *A&A*, 266, 605
- Harris, A. W., & Sonneborn, G. 1987, in *Exploring the Universe with the IUE Satellite*, ed. Y. Kondo, W. Wamsteker, A. Boggess, M. Grewing, C. de Jager, A. L. Lane, J. L. Linsky, & R. Wilson (Dordrecht: Reidel), p. 729
- Hartmann, J. 1904, *ApJ*, 19, 268
- Harvey, A. S., Stickland, D. J., Howarth, I. D., & Zuiderwijk, E. J. 1987, *Observatory*, 107, 205
- Heintz, W. D. 1980, *ApJS*, 44, 111
- Hogan, C. J. 1998, *Space Sci. Rev.*, 84, 127
- Howk, J. C., Savage, B. D. and Fabian, D. 1999, in preparation
- Humphreys, R. M. 1978, *ApJS*, 38, 309
- Hurwitz, M., Bowyer, S., Bristol, R., Dixon, W. V., Dupuis, J., Edelstein, J., Jelinsky, P., Sasseen, T. P., & Siegmund, O. 1998, *ApJ*, 500, L1
- Jenkins, E. B. 1970, in *Ultraviolet Stellar Spectra and Related Ground-Based Observations*, ed. L. Houziaux & H. Butler (Dordrecht: Reidel), p. 281
- 1971, *ApJ*, 169, 25
- 1996, *ApJ*, 471, 292
- Jenkins, E. B., & Peimbert, A. 1997, *ApJ*, 477, 265
- Jenkins, E. B., Savage, B. D., & Spitzer, L. 1986, *ApJ*, 301, 355
- Jenkins, E. B., Joseph, C. L., Long, D., Zucchini, P. M., Carruthers, G. R., Bottema, M., & Delamere, W. A. 1988, in *Ultraviolet Technology II*, ed. R. E. Huffman (Bellingham: The International Society for Optical Engineering), p. 213
- Jenkins, E. B., Reale, M. A., Zucchini, P. M., & Sofia, U. J. 1996, *Ap&SS*, 239, 315

- Jura, M. 1982, in *Advances in Ultraviolet Astronomy: Four Years of IUE Research*, ed. Y. Kondo & J. M. Mead (Greenbelt: NASA), p. 54
- Koch, R. H., & Hrivnak, B. J. 1981, *ApJ*, 248, 249
- Lampton, M., Margon, B., & Bowyer, S. 1976, *ApJ*, 208, 177
- Laurent, C., Vidal-Madjar, A., & York, D. G. 1979, *ApJ*, 229, 923
- Lemoine, M., Vidal-Madjar, A., Bertin, P., Ferlet, R., Gry, C., & Lallement, R. 1996, *A&A*, 308, 601
- Linsky, J. L., & Wood, B. E. 1996, *ApJ*, 463, 254
- Linsky, J. L., Diplas, A., Wood, B. E., Brown, A., Ayres, T. R., & Savage, B. D. 1995, *ApJ*, 451, 335
- Massa, D., Van Steenberg, M. E., Oliverson, N., & Lawton, P. 1998, in *Ultraviolet Astrophysics Beyond the IUE Final Archive*, ed. W. Wamsteker & R. Gonzalez Riestra (Noordwijk: ESA), p. 723
- McAlister, H. A., & Hendry, E. M. 1982, *ApJS*, 49, 267
- McCullough, P. R. 1992, *ApJ*, 390, 213
- Meier, R. R. 1991, *Space Sci. Rev.*, 58, 1
- Meyer, D. M., Cardelli, J. A., & Sofia, U. J. 1997, *ApJ*, 490, L103
- Meyer, D. M., Jura, M., & Cardelli, J. A. 1998, *ApJ*, 493, 222
- Meyer, D. M., Jura, M., Hawkins, I., & Cardelli, J. A. 1994, *ApJ*, 437, L59
- Morton, D. C. 1991, *ApJS*, 77, 119
- Murray, M. J., Dufton, P. L., Hibbert, A., & York, D. G. 1984, *ApJ*, 282, 481
- Olive, K. A., Schramm, D. N., Steigman, G., & Walker, T. P. 1990, *Physics Letters B*, 236, 454
- Piskunov, N., Wood, B. E., Linsky, J. L., Dempsey, R. C., & Ayres, T. R. 1997, *ApJ*, 474, 315
- Press, W. H., Teukolsky, S. A., Vetterling, W. T., & Flannery, B. P. 1992, *Numerical Recipes in Fortran*, 2nd ed., (Cambridge: Cambridge Univ. Press)
- Reeves, H., Audouze, J., Fowler, W. A., & Schramm, D. N. 1973, *ApJ*, 179, 909
- Rogerson, J. B., Spitzer, L., Drake, J. F., Dressler, K., Jenkins, E. B., Morton, D. C., & York, D. G. 1973, *ApJ*, 181, L97
- Routly, P. M., & Spitzer, L. 1952, *ApJ*, 115, 227

- Rugers, M., & Hogan, C. J. 1996, *AJ*, 111, 2135
- Savage, B. D., & Sembach, K. R. 1991, *ApJ*, 379, 245
- Savage, B. D., Bohlin, R. C., Drake, J. F., & Budich, W. 1977, *ApJ*, 216, 291
- Scully, A., Cassé, M., Olive, K. A., & Vangioni-Flam, W. 1997, *ApJ*, 476, 521
- Sembach, K. R., & Danks, A. C. 1994, *A&A*, 289, 539
- Shull, J. M., & Van Steenberg, M. E. 1985, *ApJ*, 294, 599
- Siluk, R. S., & Silk, J. 1974, *ApJ*, 192, 51
- Smith, M. S., Kawano, L. H., & Malaney, R. A. 1993, *ApJS*, 85, 219
- Sofia, U. J., Cardelli, J. A., & Savage, B. D. 1994, *ApJ*, 430, 650
- Sofia, U. J., & Jenkins, E. B. 1998, *ApJ*, 499, 951
- Songaila, A., Cowie, L. L., Hogan, C. J., & Rugers, M. 1994, *Nat*, 368, 599
- Sonneborn, G., et al. 1999, in preparation
- Spitzer, L., Cochran, W. D., & Hirshfeld, A. 1974, *ApJS*, 28, 373
- Steigman, G., & Tosi, M. 1992, *ApJ*, 401, 150
- 1995, *ApJ*, 453, 173
- Timmes, F. X., Truran, J. W., Lauroesch, J. T., & York, D. G. 1997, *ApJ*, 476, 464
- Tosi, M., Steigman, G., Matteucci, F., & Chiappini, C. 1998, *ApJ*, 498, 226
- Tytler, D., Burles, S., Lu, L., Fan, X.-M., Wolfe, A., & Savage, B. D. 1999, *AJ*, 117, 63
- Vallerga, J. V., Vedder, P. W., Craig, N., & Welsh, B. Y. 1993, *ApJ*, 411, 729
- Vidal-Madjar, A., & Gry, C. 1984, *A&A*, 138, 285
- Vidal-Madjar, A., Laurent, C., Bruston, P., & Audouze, J. 1978, *ApJ*, 223, 589
- Vidal-Madjar, A., Ferlet, R., Laurent, C., & York, D. G. 1982, *ApJ*, 260, 128
- Vidal-Madjar, A., Lemoine, M., Ferlet, R., Hébrard, G., Koester, D., Audouze, J., Cassé, M., Vangioni-Flam, E., & Webb, J. 1998, *A&A*, 338, 694
- Wampler, E. J., Williger, G. M., Baldwin, J. A., Carswell, R. F., Hazard, C., & McMahon, R. G. 1996, *A&A*, 316, 33
- Watson, W. D. 1973, *ApJ*, 182, L73
- Webb, J. K., Carswell, R. F., Lanzetta, K. M., Ferlet, R., Lemoine, M., Vidal-Madjar, A., & Bowen, D. V. 1997, *Nat*, 388, 250
- Wood, B. E., Alexander, W. R., & Linsky, J. L. 1996, *ApJ*, 470, 1157

Wood, B. E., & Linsky, J. L. 1998, ApJ, 492, 788

Wright, C. M., van Dishoeck, E. F., Cox, P., Sidher, S. D. and Kessler, M. F. 1999, ApJ, in press

York, D. G., & Jura, M. 1982, ApJ, 254, 88

York, D. G., Spitzer, L., Bohlin, R. C., Hill, J., Jenkins, E. B., Savage, B. D., & Snow, T. P. 1983, ApJ, 266, L55